Agricultural and Forest Meteorology 259 (2018) 131–140

Contents lists available at ScienceDirect

Agricultural and Forest Meteorology

journal homepage: www.elsevier.com/locate/agrformet

Spatiotemporal pattern of terrestrial evapotranspiration in China during the past thirty years

Xiangyi Li[a], Yue He[a], Zhenzhong Zeng[a], Xu Lian[a], Xuhui Wang[a,b], Mingyuan Du[c], Gensuo Jia[d], Yingnian Li[e], Yaoming Ma[f,g], Yanhong Tang[h], Weizhen Wang[i], Zhixiang Wu[j], Junhua Yan[k], Yitong Yao[a], Philippe Ciais[b], Xianzhou Zhang[l], Yiping Zhang[m], Yu Zhang[n], Guangsheng Zhou[o], Shilong Piao[a,f,g,*]

[a] Sino-French Institute for Earth System Science, College of Urban and Environmental Sciences, Peking University, Beijing, 100871, China
[b] Laboratoire des Sciences du Climat et de l'Environnement, CEA CNRS UVSQ, Gif-sur-Yvette, 91191, France
[c] Institute for Agro-Environmental Sciences, National Agriculture and Food Research Organization, Tsukuba, 305-8604, Japan
[d] CAS Key Laboratory of Regional Climate-Environment for Temperate East Asia, Institute of Atmospheric Physics, Chinese Academy of Sciences, Beijing, 100029, China
[e] Key Laboratory of Adaptation and Evolution of Plateau Biota, Northwest Institute of Plateau Biology, Chinese Academy of Sciences, Xining, 810008, China
[f] Key Laboratory of Alpine Ecology and Biodiversity, Institute of Tibetan Plateau Research, Chinese Academy of Sciences, Beijing, 100085, China
[g] Center for Excellence in Tibetan Earth Science, Chinese Academy of Sciences, Beijing, 100085, China
[h] Department of Ecology, College of Urban and Environmental Sciences, Peking University, Beijing, 100871, China
[i] Northwest Institute of Eco-Environment and Resources, Heihe Remote Sensing Experimental Research Station, Chinese Academy of Sciences, Lanzhou, 730000, China
[j] Rubber Research Institute, Chinese Academy of Tropical Agricultural Sciences, Danzhou, 571737, China
[k] South China Botanical Garden, Chinese Academy of Sciences, Guangzhou, 510650, China
[l] Key Laboratory of Ecosystem Network Observation and Modeling, Institute of Geographic Sciences and Natural Resources Research, Chinese Academy of Sciences, Beijing, 100101, China
[m] Key Laboratory of Tropical Forest Ecology, Xishuangbanna Tropical Botanical Garden, Chinese Academy of Sciences, Mengla, Yunnan, 666303, China
[n] Cold and Arid Regions Environmental and Engineering Research Institute, Chinese Academy of Sciences, Lanzhou, 730000, China
[o] State Key Laboratory of Vegetation and Environmental Change, Institute of Botany, Chinese Academy of Sciences, Beijing, 100093, China

ARTICLE INFO

Keywords:
China
Eddy covariance
Evapotranspiration
Model tree ensemble (MTE)
Spatio-temporal change
Land surface model

ABSTRACT

Evapotranspiration (ET) is one of the most important fluxes in terrestrial ecosystems that regulate atmosphere–hydrosphere–biosphere interactions. Several studies have suggested that global ET has significantly increased in the past several decades, and that such increase has exhibited big spatial variability, but there are few detailed studies on the spatio-temporal change in ET over China. Here, we developed a high-resolution data-oriented monthly ET product in China between 1982 and 2015 by integrating remote-sensing and the eddy covariance technique observed ET data in a machine learning approach (model tree ensemble, MTE). We showed that the mean annual ET over China is 552 ± 14 mm yr^{-1}, which is comparable to the estimate from a MTE-derived product based on water balance, but is larger than that from both previous MTE-derived global product and process-based land surface models. ET in China significantly increased with a rate of 10.7 mm yr^{-1} per decade over the past 30 years ($p < 0.05$). The largest increases in ET (> 60 mm yr^{-1} per decade) occurred in the eastern periphery of Sichuan, southern Taiwan, and central China, which was attributed to the increases in temperature and solar radiation, as well as the enhanced vegetation productivity. About 22% of the area showed a decreasing trend in ET, mainly in parts of southeastern, southwestern, and northeastern China. The regional decrease in ET was likely due to decreasing precipitation and/or vegetation browning. Although our finding of the significant increase in China's ET at the country scale is supported by five different ET products, there are still less agreement on the change in ET at the regional scale among different ET products.

1. Introduction

Terrestrial evapotranspiration (ET) is an important flux in the global ecosystem that links water, energy, and carbon cycles (Sellers et al., 1997; Trenberth et al., 2007; Wang and Dickinson, 2012). There is a general consensus that global annual ET has increased significantly

* Corresponding author at: Sino-French Institute for Earth System Science, College of Urban and Environmental Sciences, Peking University, Beijing 100871, China.
E-mail addresses: slpiao@pku.edu.cn, ShiLong.Piao@lsce.ipsl.fr (S. Piao).

https://doi.org/10.1016/j.agrformet.2018.04.020
Received 14 September 2017; Received in revised form 28 January 2018; Accepted 29 April 2018
Available online 04 May 2018
0168-1923/

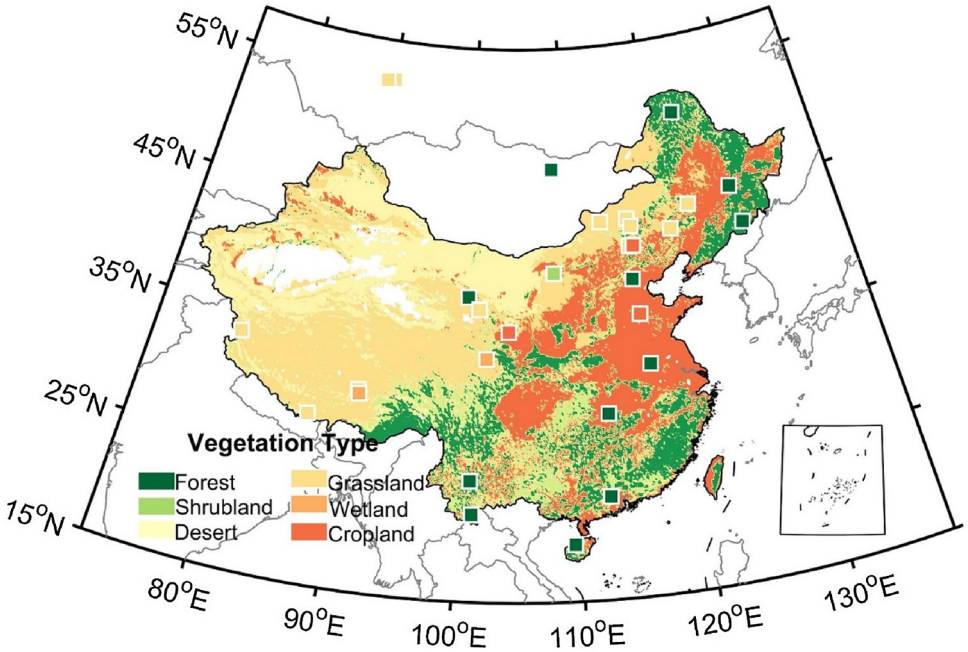

Fig. 1. Distribution of the 36 eddy covariance tower sites used in this study. Background colour shows the vegetation type: forest, shrubland, desert, grassland, wetland, and cropland.

under the impacts of climate change and human activities over the past three decades (Jung et al., 2010; Douville et al., 2012; Mueller et al., 2013; Zeng et al., 2012, 2014). However, large uncertainty still exists in the magnitude and even the sign of the ET trend at the regional scale (Jung et al., 2010; Miralles et al., 2014; Zeng et al., 2012, 2014), which refers to a national basis in this study. ET estimation can be quite different with inconsistent forcing data (e.g. sources, resolutions, accuracy, processing methods (Mueller et al., 2013; Badgley et al., 2015) and different models that can have divergent performance associated with model structures and parameterization schemes (Pan et al., 2015). In addition, the limited global long-term observations impede us to validate the model estimation and understand the potential mechanisms (Chen et al., 2014; Mao et al., 2015). Such uncertainty leads to some disagreements about spatial and temporal characteristics of ET, such as the regional ET trend as well as its drivers. Reducing uncertainty in the regional ET variation is one of the prioritized studies of the water cycle, carbon cycle, land–atmosphere interaction, as well as water management (Kustas and Norman, 1996; Bastiaanssen, 2000; Mueller et al., 2013; Jasechko et al., 2013). Previous studies attempted to reduce uncertainty by different approaches, such as applying more direct observations and integrating multiple models (e.g., Yao et al., 2017)

Several approaches have been used to investigate the global ET change based on a combination of satellite and ground observations (Mu et al., 2007; Jung et al., 2010; Zhang et al., 2010; Mu et al., 2011; Yan et al., 2012; Zeng et al., 2012, 2014). In particular, data-driven models have been applied to generate a global ET dataset using the eddy covariance measurements (Jung et al., 2009, 2010). Unlike process-driven land surface models that are complex and subject to uncertainty from model-specific structure and parameter schemes (Pan et al., 2015; Rigden and Salvucci, 2015; Yao et al., 2017), this data-driven method depends less on theoretical and empirical assumptions. In addition, the eddy covariance technique provides direct observations of ET at the site level, whereas the flux tower is not uniformly distributed and very few flux sites are available over some climate change hotspot regions (e.g., tropical and arctic regions). This inhomogeneous distribution results in large uncertainties in ET estimates at both regional and global scales. China encompasses a wide range of climate and vegetation types; yet, only nine flux tower sites in China have been used in the global ET dataset reconstructed using the eddy covariance technique (Jung et al., 2010). This could lead to a large uncertainty in the global and China ET estimates.

In this study, we collected observations from 36 flux tower sites covering almost all ecosystem types in China and applied model tree ensemble (MTE) algorithms to reconstruct a monthly ET dataset over China with a spatial resolution of 0.1° from 1982 to 2015. The MTE method has been proven to be robust of extrapolating ET to the regions not covered by eddy covariance towers (Jung et al., 2010). Compared with the sophisticated models, this empirical method links the ET to various driving variables that can be obtained easily (Zhang et al., 2016a). This method is complementary to process-based models because there is a large spread in current model estimates of ET (Jung et al., 2011). We improved the China's ET estimates through using more in-situ measurements, eliminating the problem of solar radiation (which is a key limitation in Jung's ET product, 2010), as well as realizing a higher spatial resolution and a longer time period.

We compared our ET estimates with global ET datasets, including a data-driven empirical model with ET measurements calculated using the eddy covariance technique (Jung et al., 2009), a data-driven empirical model with ET observations from terrestrial water balance (Zeng et al., 2014), and three datasets from process-based land surface models (the Community Atmosphere Biosphere Land Exchange (CABLE), (Wang et al., 2010b); the Organizing Carbon and Hydrology In Dynamic Ecosystems Environment (ORCHIDEE), Krinner et al., 2005; and the Version 4 of the Community Land Model with coupled Carbon and Nitrogen cycles (CLM4CN), Oleson et al., 2010). We discussed the uncertainty and limitations of ET products through comparing the spatial and temporal characteristics of ET.

2. Material and methods

2.1. Data sources

2.1.1. Data from the eddy covariance flux tower sites

The global network of micrometeorological flux measurement sites (FLUXNET) provides ground measurements of carbon, water, and energy fluxes, as well as meteorological, plant, and soil data, on a continuous and long-term basis (Baldocchi et al., 2001). The eddy

Table 1
The information of ET products used in this study.

Product name	Time period	ET schemes	General method	Advantages	Limitations	Citation
FLUX-MTE	1982–2011	Eddy covariance method; Model Tree Ensemble (MTE)	Data-driven	Simple to apply; based on observations	Neglecting solar radiation, wind speed and humidity; limited observed data	Jung et al. (2010, 2011)
WB-MTE	1982–2009	Water balance method; Model Tree Ensemble (MTE)	Data-driven	Not require any model assumption; based on situ discharge measurements	Counting for the evaporation from rivers and lakes; large uncertainties in wet season and tropical regions	Zeng et al. (2014)
CABLE	1982–2010	Water vaporization is a function of surface temperature; transpiration is calculated using two-leaf approach (Wang and Leuning, 1998); and soil evaporation is calculated following (Decker et al., 2017)	Process-based	Based on the solid theoretical basis and representing sophisticated physical processes	Uncertainty from input data, model structure and parameterizations; commonly underestimating transpiration	Wang et al. (2010b)
ORCHIDEE	1982–2012	Partitioning ET into bare soil evaporation (decreases with soil moisture in the top layer), interception loss and transpiration (controlled by a stomatal conductance, Guimberteau et al., 2014)	Process-based			Krinner et al. (2005)
CLM4CN	1982–2009	Partitioning ET into ground evaporation, canopy evaporation and transpiration; dependent on plant function types (PFTs).	Process-based			Oleson et al. (2010)

covariance data used in this study were obtained from global FLUXNET (http://fluxnet.fluxdata.org), AsiaFlux (http://www.asiaflux.net), and ChinaFlux (http://www.chinaflux.org/enn/index.aspx) datasets. Fig. 1 shows the spatial distribution of the 36 flux tower sites used in this study. The tower sites were located in and around China with good geographical and vegetation diversity. They distributed over five vegetation types: forest, shrubland, grassland, wetland, and cropland. There were in total 12 flux tower sites covered by forests, including deciduous broadleaf forests (DBF, 4 sites), deciduous needle-leaf forests (DNF, 3 sites), evergreen broadleaf forests (EBF, 2 sites), evergreen needle-leaf forests (ENF, 2 sites), and mixed forests (MF, 1 site). The half-hourly ground-measured data, including precipitation, temperature, incoming solar radiation, relative humidity, and ET were processed under gap-filled and quality control following the standardized techniques described in previous studies (Reichstein et al., 2005; Moffat et al., 2007; Jung et al., 2009). Last, the data were aggregated to a monthly scale. In total, 826 site-month flux records were collected during 2002–2014 for this study. Details of the eddy flux tower sites are shown in Table A1.

2.1.2. Satellite-derived normalized difference vegetation index data

The Advanced Very High Resolution Radiometer (AVHRR) instruments provide a long record (from 1981 to present) of the normalized difference vegetation index (NDVI). The $NDVI_{3g}$ global dataset used in this study, produced by the Global Inventory Modeling and Mapping Studies at NASA/Goddard Space Flight Center (Tucker et al., 2005; Pinzon and Tucker, 2014), is an improved AVHRR-based NDVI dataset with spatial resolution of 1/12 × 1/12° and a 15-day interval temporal resolution. It is of high quality and has been widely used in studies on vegetation dynamics (e.g., Piao et al., 2006; Pinzon and Tucker, 2014). We extracted China's NDVI data from the global $NDVI_{3g}$ dataset, aggregated the data within a month by obtaining the maximum NDVI value from semi-monthly values (Pinzon and Tucker, 2014), and aggregated the data to 0.1° grids using block averaging method (Zhang et al., 2017).

2.1.3. Meteorological data

The climate variables used in this study include surface air temperature, precipitation, incoming solar radiation, and relative humidity (Table A2). We downloaded these climate variables from the China Meteorological Forcing Dataset (http://westdc.westgis.ac.cn/data/7a35329c-c53f-4267-aa07-e0037d913a21) at a 0.1° × 0.1° spatial resolution and a monthly time step during 1982–2015. The dataset was developed by the hydrometeorological research group at the Institute of Tibetan Plateau Research, Chinese Academy of Sciences by merging a variety of data sources, including China Meteorological Administration station measurements, Tropical Rainfall Measuring Mission 3B42 precipitation analysis data, the Global Energy and Water-Cycle Experiment–Surface Radiation Budget shortwave radiation data set, Global Data Assimilation System atmospheric reanalysis data, and Princeton reanalysis data (Yang et al., 2010; Chen et al., 2011).

2.1.4. Vegetation distribution map

The vegetation distribution map used in this study is a 1:1000,000 digitalized vegetation map of China (Editorial Board of Vegetation Map of China, Chinese Academy of Sciences (EBVMC), 2007). We reclassified the 573 vegetation types in the map into six categories: forest, shrubland, desert, grassland, cropland, and wetland (Fig. 1).

Forest was reclassified into five plant functional types for the training of MTE with eddy covariance measurements and the generation of ET products, including DNF, DBF, EBF, ENF, and MF. Grassland includes cool season (C3) grasses and warm season (C4) grasses, which have quite different photosynthetic capacity due to their different photosynthetic pathways (Winslow et al., 2003). ET of C3 and C4 grasses differ in ET because the evaporative loss rate is coupling to carbon uptake (Ukkola and Prentice, 2013). We did not separate C3 and

C4 grasses because the latter only occupies 1.3% of China's grasslands (https://webmap.ornl.gov/ogc/dataset.jsp?ds_id = 20042, Wei et al., 2014). In addition, there is no C4 grasses site included for the MTE training. Our result shows that the lack of C4 grasses sites data led to very weak bias in the estimated ET (Fig. A1g)

2.1.5. ET products

We compared the spatiotemporal characteristics of ET change in our ET dataset with five global ET products at 0.5° spatial resolution and a monthly temporal resolution, including two data-driven ET products and three model-based ET products (Table 1). The data-driven models are constructed based on the relationship between the target variable and multiple explanatory variables. They don't rely on any theoretical assumption, and are largely determined by the quality, quantity and representativeness of forcing data. One data-driven global ET product (1982–2011) was generated by Jung et al. (2010, 2011) by integrating flux measurements and the MTE algorithm (hereafter FLUX-MTE) and the other data-driven global ET product (1982–2009) was created by Zeng et al. (2012, 2014) by coupling water balance (WB) observations with MTE (hereafter WB-MTE). The process-based models simulate different physical processes that control ET to isolate the effect of different driving factors. They can reveal the underlying mechanisms of ET process. Three model-based ET products were derived from three land surface models, including CABLE (Wang et al., 2010b), ORCHIDEE (Krinner et al., 2005), and CLM4CN (Oleson et al., 2010). The ET products from CABLE (1982–2010) and ORCHIDEE (1982–2012) are driven by varying climate and atmospheric CO2 concentrations, and that from CLM4CN (1982–2009) is driven by varying climate, atmospheric CO2 concentration, and nitrogen deposition (Huang et al., 2015).

2.2. Methods

2.2.1. MTE for the ET estimate

We applied the MTE algorithm proposed by Jung et al. (2009, 2010, 2011) to generate gridded ET in China at a 0.1° spatial resolution and monthly temporal resolution from 1982 to 2015. The MTE algorithm is an empirical method that predicts ET based on a set of explanatory variables (Table A3) according to model trees trained with the FLUXNET eddy covariance measurements. Note that vegetation type is an important variable for data stratification. Nine different vegetation types were applied here, including DNF, DBF, EBF, ENF, MF, grassland, cropland, shrubland, and wetland. We first constructed 1000 model trees at the site level and selected 25 best-independent trees with the minimum Bayesian information criterion for the prediction. We applied the established MTE for empirical upscaling over all of China using the gridded datasets of the same explanatory variables as those used for training at the site level. Previous studies have demonstrated that MTE has good capacity to predict the target variables robustly even in regions not captured by the training data (Jung et al., 2010; Zeng et al., 2014).

2.2.2. Performance of the MTE

To evaluate the performance of the MTE algorithm in reproducing ET, we compared the MTE-derived ET estimates with the ET measurements at the 36 eddy covariance tower sites (Fig. 1). The ET measurements were separated into two parts by the way of sampling without replacement, one for model training and the other for model validation (10% of the dataset), respectively. The training data and validating data don't share any replicates. We attempted to capture more details of ET using adequate training data. Meanwhile, we tried to verify the reliable of the MTE algorithm using residual data from training data. The results revealed high coherence between MTE-derived ET and flux-observed ET for both the training data ($R^2 = 0.95$, $p < 0.01$, root mean square error [RMSE] = 0.3 mm day^{-1}, Fig. 2a) and the validating data ($R^2 = 0.87$, $p < 0.01$, RMSE = 0.5 mm day^{-1}, Fig. 2b). We further assessed the performance of the MTE algorithm for nine specific vegetation types (DBF, DNF, EBF, ENF, MF, cropland, grassland, shrubland, and wetland). The result shows that the MTE algorithm can capture ET well for all the nine different vegetation types (Fig. A1). This suggests that the MTE algorithm is capable of characterizing the spatiotemporal variations of regional ET, thus enabling derivation of reliable long-term gridded ET projections over China.

2.2.3. Trend analysis

The temporal trends in ET and its driving variables were estimated by Theil–Sen robust linear regression and tested with the Mann–Kendall (MK) non-parametric test. The Theil–Sen estimator is a non-parametric median-based slope estimator that is robust against outliers. It has been widely used to estimate ET trends by previous studies (Mueller et al., 2013; Zhang et al., 2015). The MK non-parametric test is a tool used to test the significance of trends in climate and environmental sciences (Machiwal and Jha, 2006). The null hypothesis of no trend in the time series will be rejected within the 95% confidence interval if the P-value is < 0.05 (Rahmani et al., 2015).

2.2.4. Comparison map profile method

In this study, we used the comparison map profile (CMP) method proposed by Gaucherel et al. (2008) to detect spatial similarity and difference in the ET trend among different ET datasets. Two similarity indices are applied in this method: one is absolute distance (D), which reflects the similarity of data value; the other is cross-correlational coefficient (CC), which reflects the spatial structure of the two images with the same size. The similarity indices are calculated by the moving window, which scan the rows and cols of two individual images, and the results are assigned to the central pixel in each moving window:

$$D = |(\bar{x} - \bar{y})| \tag{1}$$

where $\bar{x}$ and $\bar{y}$ are averages computed over pixels in the moving windows of two images to be compared.

$$CC = \frac{1}{N^2} \sum_{i=1}^{N} \sum_{j=1}^{N} \frac{(x_{ij} - \bar{x}) \times (y_{ij} - \bar{y})}{\sigma_x \times \sigma_y}, \tag{2}$$

$$\text{with } \sigma_x = \sqrt{\frac{1}{N^2 - 1} \sum_{i=1}^{N} \sum_{j=1}^{N} (x_{ij} - \bar{x})^2}, \tag{3}$$

where x_{ij} and y_{ij} are the pixel values at row i and column j of the two moving windows for comparison, respectively. N is total pixels in each moving window.

We aggregated the ET datasets into a uniform spatial resolution (0.5° × 0.5°) using block averaging method to meet the resolution requirements of the compared images. We generated mono-scale (4–20 spatial scales) similarity maps (the absolute distance map and the correlation map), through calculating the similarity indices with the window size varying from 9 × 9 pixels (represented by scale 4) to 41 × 41 pixels (represented by scale 20) for the compared images. According, the final multi-scale similarity maps (averaging the mono-scale maps) are determined by the information from different scales. The 1–3 scales (from 3 × 3 pixels to 7 × 7 pixels) mono-scale similarity maps are not included in order to avoid biases at very small window size, because the similarity indices in these scales changed sharply (Fig. A2). The similarity indices decrease to small values when the window size reaches to the scale 20 (41 × 41 pixels) and no more information can be captured by larger window sizes (Fig. A2), so the larger scales (> scale 20) are also excluded. High similarities between the two compared images are indicated by a low D and/or high CC, whereas high differences are indicated by a high D and/or low CC. Detailed information on CMP method can be found in Gaucherel et al.'s paper (2008).

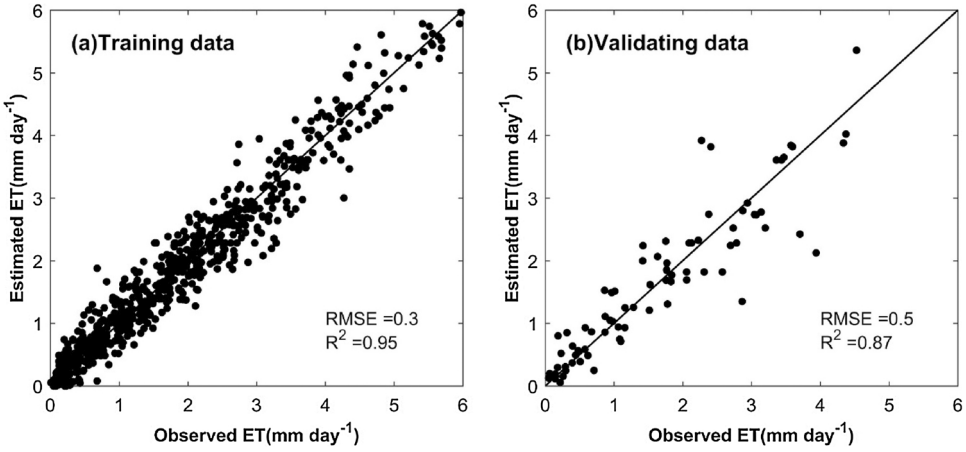

Fig. 2. Comparison between model tree ensemble (MTE)-estimated evapotranspiration (ET) and eddy covariance observations. (a) Training data (R^2 = 0.95, root mean square error [RMSE] = 0.3 mm day^{-1}), (b) Validation data (R^2 = 0.87, RMSE = 0.5 mm day^{-1}).

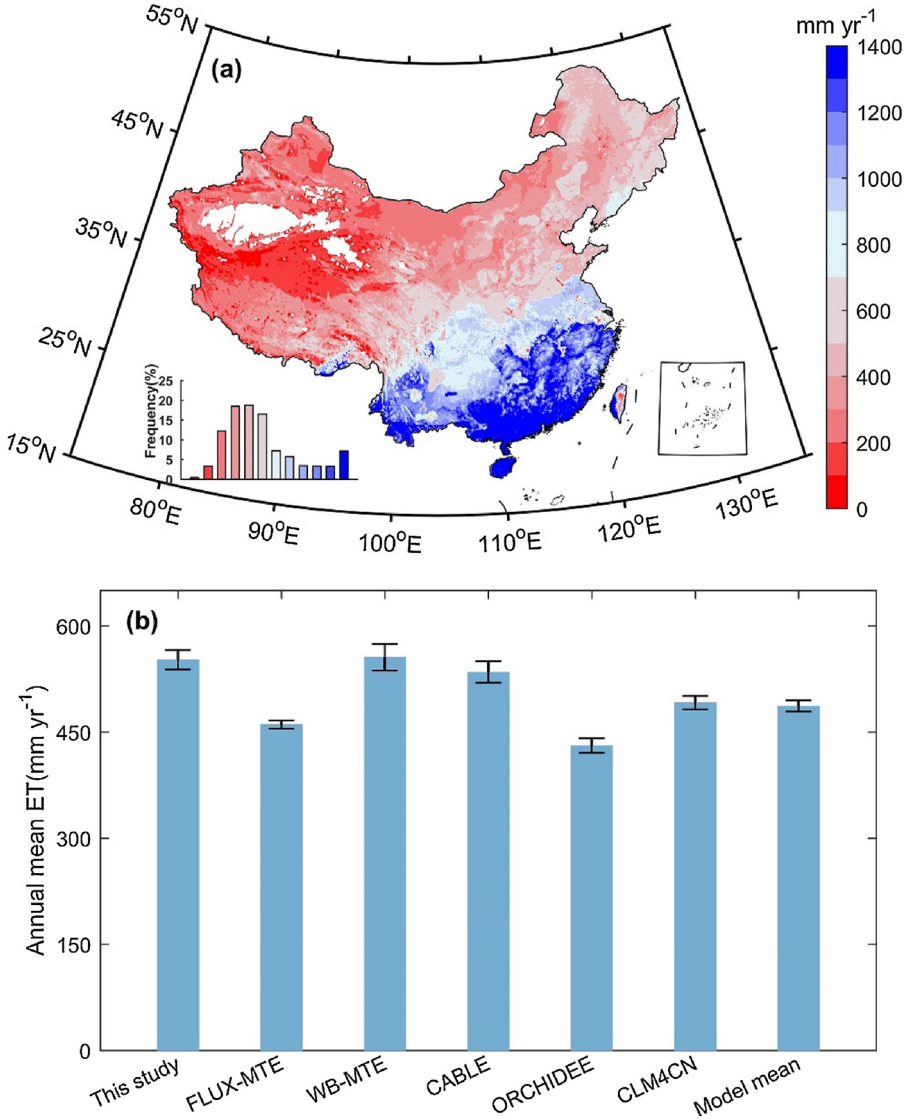

Fig. 3. (a) Spatial pattern of multi-year (1982–2015) and average mean annual ET over China. Inset denotes the frequency distribution of ET. (b) Mean annual ET averaged over the country from the datasets in this study (FLUX-MTE, WB-MTE, CABLE, ORCHIDEE, CLM4CN, and the model mean). Error bars denote the interannual variability in mean annual ET during the study period.

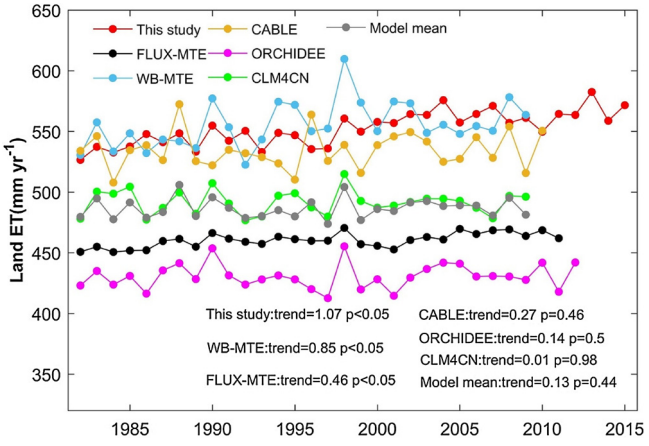

Fig. 4. Inter-annual variations in ET from the datasets in this study (1982–2015), FLUX-MTE (1982–2011), WB-MTE (1982–2009), CABLE (1982–2010), ORCHIDEE (1982–2012), CLM4CN (1982–2009), and the model mean (1982–2009). The inserted numbers show the linear temporal trends (mm yr^{-1} per year). The annual ET value is calculated from the average ET for the whole China.

3. Results

3.1. Mean annual ET in China

The spatial pattern of the mean annual ET exhibited a notable decreasing gradient from the southeast to the northwest (Fig. 3a). The ET values across the majority of China's vegetated areas (> 63%) ranged in magnitude from 200 to 800 mm yr^{-1}. High ET values (> 1200 mm yr^{-1}) mainly distributed in humid and dense vegetation regions, including the Middle-Lower Yangtze Plain, the Pearl River Delta, the Yunnan-Guizhou Plateau, the southeastern Tibetan Plateau, the Hainan Island, and western Taiwan Island. In contrast, ET values were relatively low over the extreme dry and sparse vegetation regions, including the northern areas of the Tibetan Plateau and the Junggar Basin (< 200 mm yr^{-1}). There is no vegetation covered in the north of Tibetan Plateau (Fig. 1), so we excluded this part in the study (Fig. 3).

Averaged over all vegetated areas, the national mean annual ET weighted by area was 552 mm yr^{-1}, with an interannual variability of 14 mm yr^{-1} during 1982–2015 (Fig. 3b). This result is almost the same as that from a MTE-derived product based on the water balance method (WB-MTE, 555 ± 19 mm $year^{-1}$ during 1982–2009). However, the other MTE-derived product (FLUX-MTE, driven by relatively limited flux observations in China) (Jung et al., 2011) not only showed the smaller magnitude of mean annul ET (16%, 460 mm yr^{-1}) but also the weaker interannual variability of the mean annual ET (57%, 6 mm yr^{-1}) in 1982–2011 in comparison to our ET estimates. In addition, process-based land surface models generally have lower mean annual ET compared with our projected ET dataset, ranging from 3% (535 ± 15 mm $year^{-1}$ during 1982–2010 for CABLE) to 22% (431 ± 10 mm $year^{-1}$ during 1982–2012 for ORCHIDEE) (Fig. 3b).

3.2. Trend in ET

3.2.1. China's annual ET trend

Our dataset showed that China's annual ET increased significantly from 527 mm yr^{-1} in 1982 to 572 mm $year^{-1}$ in 2015 at a rate of 10.7 mm yr^{-1} per decade (~2% per decade, $p < 0.05$) during the study period (red line in Fig. 4). This significant and positive ET trend has been captured by global data-driven ET products, i.e., WB-MTE (8.5 mm yr^{-1} per decade, $p < 0.05$) and FLUX-MTE (4.6 mm yr^{-1} per decade, $p < 0.05$). In addition, interannual variability in China's annual ET was diagnosed by two global data-driven products ($p < 0.05$). However, the magnitude of China's ET increase was 31% higher than that of WB-MTE (1982–2009), and seriously higher (58%) than that of FLUX-MTE (1982–2011). In addition, all of the model-based ET products failed to capture the significant and positive ET trend over China during the past 30 years, as all these products showed weak and insignificant positive trends in China's annual ET (CABLE, 2.7 mm yr^{-1} per decade, $p = 0.46$; ORCHIDEE, 1.4 mm yr^{-1} per decade, $p = 0.50$; and CLM4CN, 0.1 mm yr^{-1} per decade, $p = 0.98$). The interannual variability in China's annual ET was not captured by these model-based products ($p > 0.05$).

Over the past 30 years, China's annual ET trend is expected to be driven by multiple environmental factors, such as precipitation, temperature, solar radiation, relative humidity, and vegetation density (e.g. NDVI) (Wang et al., 2010a; Shi et al., 2013). During this period, our mean annual precipitation, temperature, and NDVI over China have significantly increased ($p < 0.05$), with a positive rate of 28.6 mm yr^{-1} per decade (4.8% per decade), 0.4 oC per decade (6.4% per decade), and 6.2×10^{-3} per decade (2.0% per decade), respectively (Fig. A3a–c). Relative humidity shows a significant decreasing trend (−0.8% per $decade^{-1}$, $p < 0.05$). Solar radiation also shows a decreasing trend but is statistically insignificant (−0.4 W m^{-2} per $decade^{-1}$, $p = 0.27$, Fig. A3d, e). The results indicate that increasing annual precipitation, temperature, and NDVI as well as the decreasing relative humidity are likely to exert positive effects on ET trend, while solar radiation may contribute little to annual increasing ET trend.

Further, the ET inter-annual variability shows divergent sensitivity to different driving factors. China's ET variability during the period 1982–2015 was significantly correlated with temperature (R = 0.47, $p < 0.05$), solar radiation (R = 0.46, $p < 0.05$), and relative humidity (R = −0.33, $p < 0.1$), indicating the important role of surface meteorological conditions for affecting China's ET variability. In order to remove the spurious effect of inter-annual trend, we detrended the time series and analyzed the correlation coefficient between the inter-annual variations of MTE-estimated ET and other ET products. Given the very weak relationship between ET and precipitation (R = 0.03, $p = 0.86$), thus precipitation may not be the reason for the ET variability; this premise is also supported by a previous study showing weak sensitivity of ET to annual precipitation in China, except in the western dry regions (Liu et al., 2016a). In addition, annual ET was also insignificantly correlated to NDVI (R = 0.13, $p = 0.5$). This indicates that vegetation makes little contribution to China's ET variability, even though extensive vegetation greening (Piao et al., 2015; Zhu et al., 2016) contributes to increasing terrestrial ET worldwide (Zhang et al., 2015, Zeng et al., 2017).

3.2.2. Spatial pattern in the ET trend over China

The pattern of the ET trend during 1982–2015 exhibited high spatial heterogeneity (Fig. 5a). The majority of the study region (78%) was dominated by an increasing trend, of which more than half (51%) was significant at the 95% confidence level. A decreasing trend was observed over the remaining regions (22%), but only a small fraction (22%) was significant ($p < 0.05$). The data-driven ET products show the consistent trend with our study (71% of land surface increased in FLUX-MTE and 72% of land surface increased in WB-MTE), while fewer areas (51%–57%) increased in the process-based ET products (Fig. A4). The largest ET increase (> 60 mm yr^{-1} per decade) occurred in the eastern periphery of the Sichuan Basin, central China, and southern Taiwan. A relatively weak ET trend (0–40 mm yr^{-1} per decade) occurred in northern China (excluding eastern parts of northeastern China), and was fragmentally distributed in southern China (e.g., southeastern and northwestern Middle-Lower Yangtze Plains and the Yunnan-Guizhou Plateau). A decreasing ET trend occurred mainly in the coastal regions of China (i.e., Hainan, the Pearl River Delta, the southern Middle-Lower Yangtze Plain, and northern Taiwan), some parts of western China, and east of the Greater Khingan Mountains. Nevertheless, there exists large regional divergence in ET trend among different ET products (Fig. 5a & Fig. A4), which is further discussed in

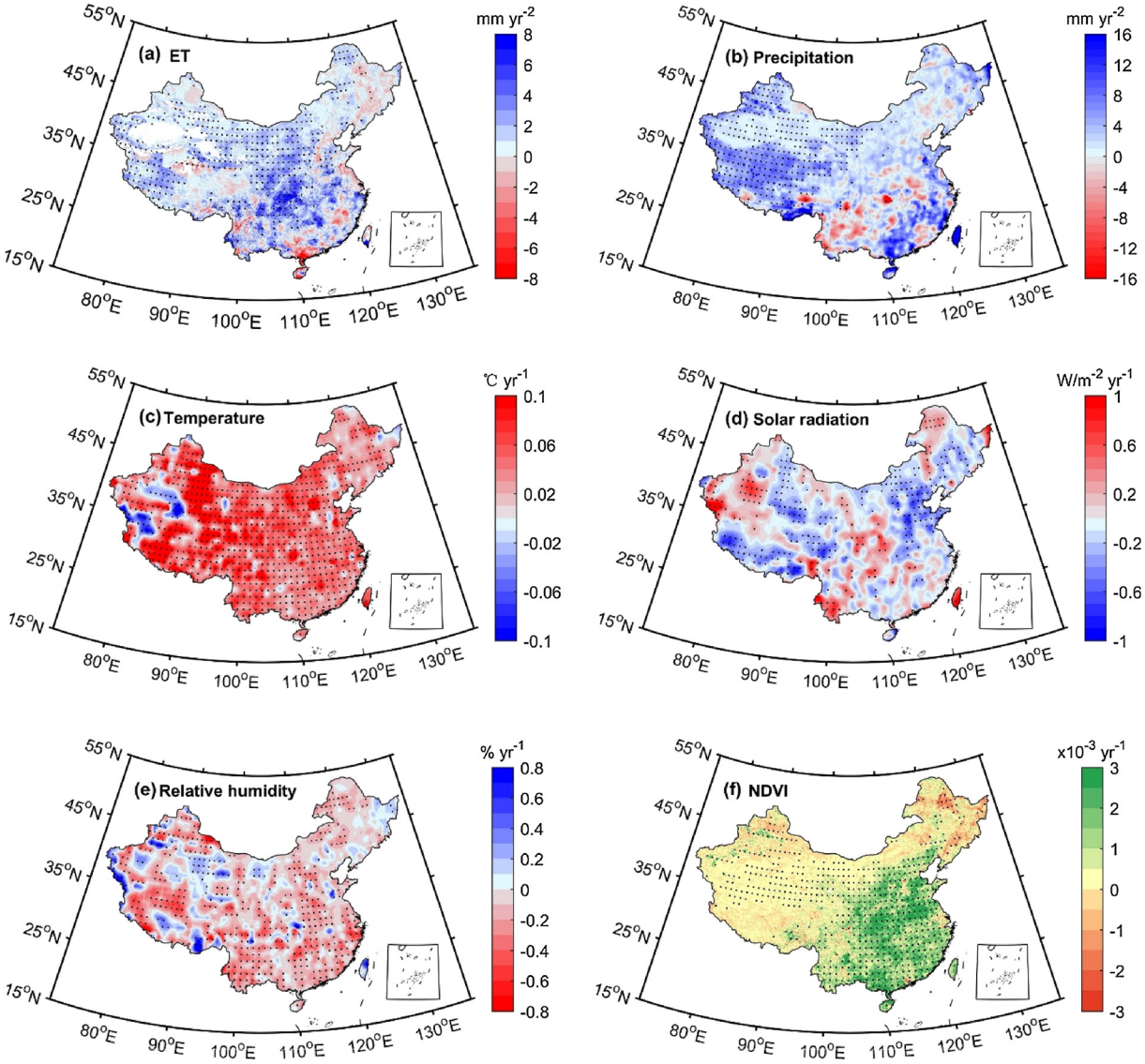

Fig. 5. Spatial patterns in the trend of (a) ET, (b) precipitation, (c) temperature, (d) solar radiation, (e) relative humidity, and (f) the normalized difference vegetation index (NDVI) during 1982–2015. Black dots indicate statistically significant trends (Mann–Kendall (MK) test: $p < 0.05$).

Section 4.2.

This large spatial heterogeneity was associated with regional changes in ET driving factors (Fig. 5b–f). Most regions experienced increasing temperature (91% of the study area, Fig. 5b), precipitation (81%, Fig. 5c), and NDVI (72%, Fig. 5d) during 1982–2015, while decreasing trends in relative humidity (71%, Fig. 5e) and solar radiation were observed (57%, Fig. 5f). Vegetation greening (i.e., increased NDVI) over China, caused by either climate change or human activities in particular China's afforestation programs (Piao et al., 2015, Liu et al., 2016b), increased annual ET. With sufficient soil moisture supply in southern China (Liu and Xie, 2013), the widespread increase of ET there is presumably attributable to the significant increase in temperature and solar radiation (Fig. 5c, d), as well as remarkable vegetation greening (i.e., increased NDVI, Fig. 5f); whereas the decreasing ET trend there is explained by the reduction of incoming solar radiation (Fig. 5d). In the area east of the Greater Khingan Mountains, the decrease in ET is presumably attributable to decrease in NDVI (Fig. 5a, f). Western China is a water-limited region; the decrease in ET in some regions is likely due to limited soil moisture, as shown by the decrease in precipitation in the Yunnan-Guizhou Plateau and the decrease in the relative humidity in the Tibetan Plateau and Junggar Basin (Fig. 4b, e).

4. Discussion

4.1. Comparison of mean annual ET among different ET products

Our results showed that ET over China varied within the range of 431–555 mm yr^{-1} in different global or regional datasets, suggesting that large uncertainties still exist in current ET estimates. This is supported by previous studies, such as Chen et al. (2014), who reported that China's ET ranges within 535–852 mm yr^{-1} according to five empirical and three process-based models. This substantial divergence is attributable to factors, such as different input datasets, model structures, and model parameterizations (Jimenez et al., 2011; Mueller et al., 2013; Zhou et al., 2012). Given that considerable uncertainties exist, we collected more flux tower sites for model training and used more representative driving factors (see Table A2) as inputs to reconstruct the regional ET over China.

Here, we used spatial correlation and RMSE to assess the spatial consistency between our dataset and the global datasets over China (Fig. 6). Our results displayed high correlation coefficients (0.85–0.99) and a discriminative RMSE of the mean annual ET ranging from 46 to 234 mm yr^{-1}. This indicated a strong spatial coherence in mean annual

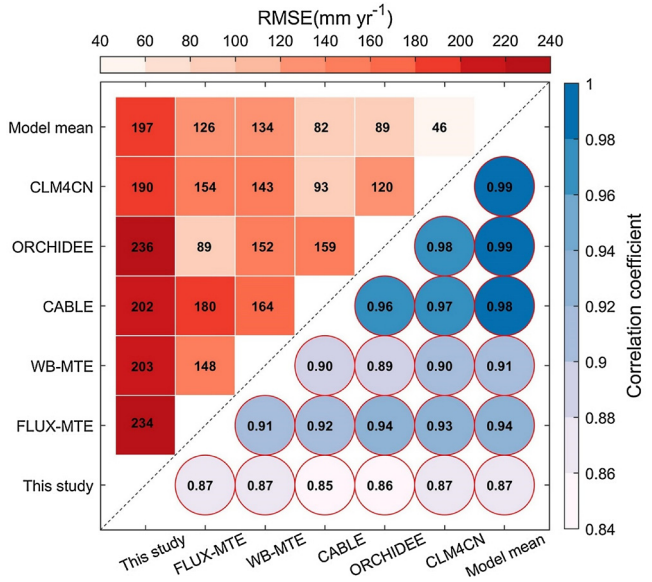

Fig. 6. Comparison of mean annual ET over China in this study with the FLUX-MTE, WB-MTE, CABLE, ORCHIDEE, CLM4CN, and the model mean during 1982 and 2009. Spatial correlation and RMSE are used to indicate the spatial coherence and magnitude, respectively. Significant correlations are shown with red edged circles (MK test: $p < 0.05$) (For interpretation of the references to colour in this figure legend, the reader is referred to the web version of this article).

ET among the different ET datasets, but the magnitudes of the ET values were substantially different (Fig. 3; Fig. A5a–f). Yet, our ET product shows more discrepancies than others, with a lower correlation and higher RMSE than inter-comparison across other ET products. The difference between our ET product and two data-driven ET products (FLUX-MTE and WB-MTE) mainly appears in Southern China, while more widespread discrepancies exist between our ET product and process-based models (Fig. 3 & Fig. A5c-f).

China's mean annual ET in FLUX-MTE is lower than our ET dataset (Fig. 3b). The reason could be the limited coverage of flux tower sites in southern China in which high ET values dominate, and they fail to consider an important driving factor (i.e., solar radiation) in their MTE framework (Jung et al., 2010; Wang and Dickinson, 2012). These deficiencies impose a profound influence on the hot and humid regions, particularly southern China, where substantial uncertainty exist in the FLUX-MTE ET dataset (Fig. 3a versus Fig. A5a). In addition, the flux tower sites used for data training primarily distributed in the northern China (Jung et al., 2010), which induced large uncertainty in southern China for the FLUX-MTE ET. WB-MTE has significantly lower ET in southwestern China than our ET product. WB-MTE is short of basin-scale ET in the southwestern China for ET training (Zeng et al., 2014), while we applied two forest flux tower sites (Xishuangbanna and Ailaoshan, Fig. 1) in this region.

China's mean annual ET is substantially lower in three widely used process-based land surface models (CABLE, ORCHIDEE, and CLM4CN) compared with our ET dataset (Fig. 3a vs. Fig. A5c–f). The process-based land surface models simulated ET processes (i.e., plant transpiration, soil evaporation, and interception loss) using priori parameter sets (e.g., soil and vegetation properties) (Kowalczyk et al., 2006; Wang et al., 2011; Ukkola et al., 2016). These priori parameters largely simplify the sophisticated biophysical processes in the real world; uncertainties in model parameterization lead to uncertainties in ET simulations. For example, previous studies reported that current land surface models underestimate the ratio of plant transpiration to total terrestrial ET (Evaristo et al., 2015); this constitutes an important source of the uncertainty in ET simulations (Zeng et al., 2017). In contrast, the MTE-estimated ET are derived based on direct site ET observations, which lead to a good performance in estimating the total amount of ET flux, even though the components of ET (i.e. plant

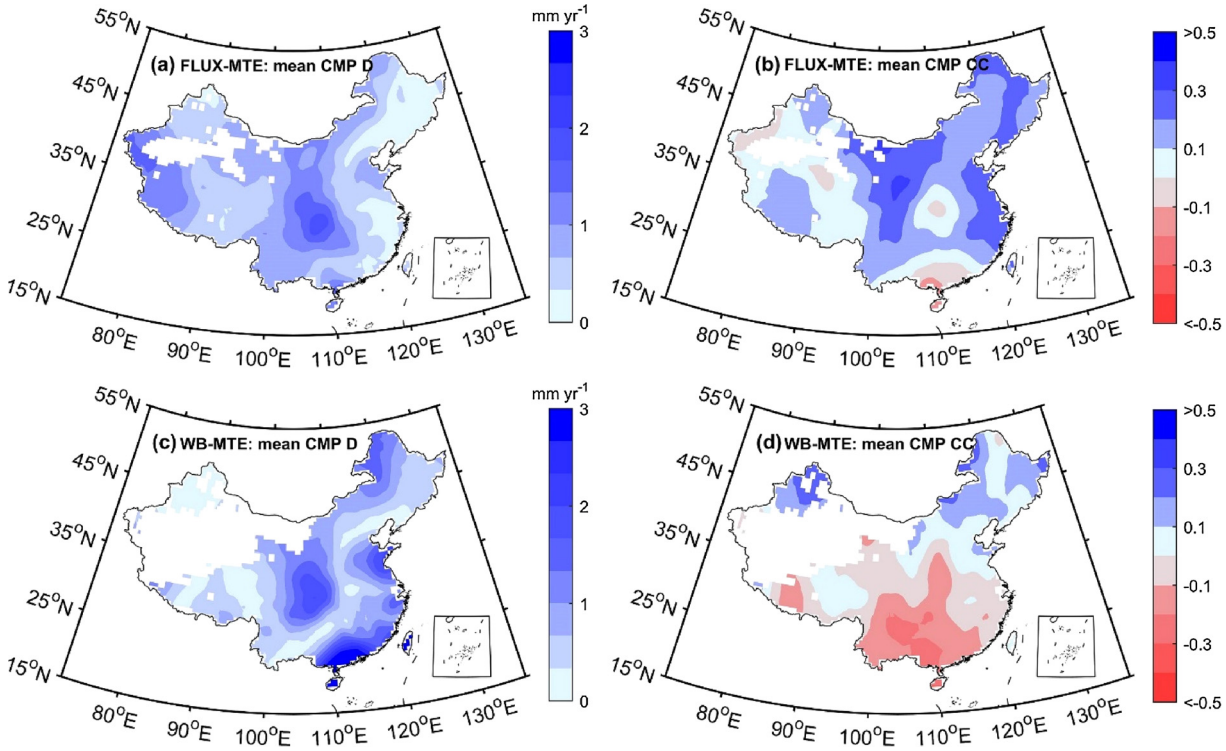

Fig. 7. Comparison of trend in the pattern of annual ET over China between the ET dataset in this study and the two global data-driven ET datasets (a, b) FLUX-MTE, (c, d) WB-MTE using the comparison map profile (CMP) method. Two indices are used: (a, c) mean CMP distance (D), and (b, d) mean CMP cross-correlational coefficient (CC). The indices were averaged over the 4–20 mono-scale similarity maps.

transpiration, soil evaporation, and interception loss) cannot be directly assessed. Current models have coarse spatial resolution, resulting in a poor capacity of the models to capture ET characteristics over specific biomes and climatic zones (Fisher et al., 2008; Mu et al., 2011; Zhang et al., 2016c), especially considering the heterogeneous landscapes across China.

Uncertainties also exist in our MTE-estimated ET product. First, C3 and C4 grasses were not differentiated in this study, which may cause some uncertainties in ET estimates over grasslands. Yet, this uncertainty could be negligible because C4 grasses mainly distribute in southeastern China and with a very small percentage (1.3%). Second, cropland is greatly impacted by human activities, such as agricultural regulation and irrigation. This effect can lead to uncertainties in estimating ET but it is difficult to assess. Meanwhile, the direct observations are still limited to capture the ET at local scale. For example, only forest flux tower sites have been applied in Southern China in this study, which overestimate ET in this region.

4.2. Comparison of ET trends among different ET products

Large discrepancies also exist among different ET datasets regarding inter-annual variability and trends in mean annual ET over China. We employed the CMP method (Gaucherel et al., 2008) to examine the similarity in the ET trend pattern over China between our ET dataset and two global data-driven ET datasets (FLUX-MTE and WB-MTE) (Fig. 7). Spatial consistency was clearly observed between the ET trends in our dataset and FLUX-MTE (mean CMP D < 0.5 mm year^{-1}, mean CMP CC > 0.3) over regions where ET is limited by water availability (e.g., the Northeast China Plain and Inner Mongolian Plateau) (Fig. 7a, b; Fig. 5a; Fig. A4a). However, a noticeable difference in the ET trend appeared in the eastern periphery of Sichuan Basin and tropical southern China (mean CMP D > 1.5 mm year^{-1}, mean CMP CC < 0, Fig. 7a, b). FLUX-MTE showed a consistent slight increase over the two regions, whereas our dataset displayed a large increase in the eastern periphery of Sichuan Basin but a decrease in tropical southern China (Fig. 5a vs. Fig. A4a). This was expected because the ET changes in our data were driven by both increasing temperature and decreasing solar radiation that compensated for each other, whereas the changes in FLUX-MTE were only controlled by increasing temperature owing to the neglect of solar radiation change in previous studies (Jung et al., 2010; Zeng et al., 2012; Wang and Dickinson, 2012).

Striking contrasts in the ET trend existed between our dataset and WB-MTE, with the hotpots of disparity (mean CMP D > 2 mm year^{-1}, mean CMP CC [-0.3–0.1]) occurring in tropical and subtropical southern China (Fig. 7c, d; Fig. 5a; Fig. A4b). The divergence may be due to the different scaling processes used for the ET reconstructions between our dataset (upscaling from the site level) and WB-MTE (downscaling from the catchment level). Because the response of ET to driving factors is scale-dependent (Jarvis, 1995), the functional relationships established between ET and driving factors may differ between our MTE framework and the WB-MTE framework. WB-MTE ET has limitations during the wet season compared with other approaches, which may have led to the divergence (Zeng et al., 2014).

In addition, we also detected similarities and differences in the sign and magnitude of the ET trend between our dataset and the model-based ET datasets over China using the CMP method (Fig. A6). The consistency between our dataset and the model-based ET products (CABLE, ORCHIDEE, and CLM4CN) mainly occurred in northwestern China (mean CMP D < 0.5 mm year^{-1}, mean CMP CC > 0.2), whereas the difference mainly appeared in central and southeastern China (mean CMP D > 2 mm year^{-1}, mean CMP CC < -0.2) (Figs. A4c–f, A6). The discrepancy could be attributed to several reasons. First, the ratio of vegetation transpiration is underestimated in land surface models. This incorrect partitioning of ET influences the sensitivity of the ET change in response to environmental factors and consequently leads to substantial divergence in the ET trend. For example, as a response of terrestrial ET to greening, a decrease in soil evaporation rather than an increase in vegetation transpiration would dominate the overall ET trend due to the underestimated vegetation transpiration in ET partitioning (Zeng et al., 2017), especially in southern China where vegetation transpiration dominates ET (Zhang et al., 2016b). Second, model parameterizations using short-term observations would invariably induce biases in the long-term variations of the model simulations, because acclimation of the vegetation to the new environmental conditions is not captured by short-term observations (Wang and Dickinson, 2012). Last, the land surface models may have limitations simulating the ET processes. For example, previous studies documented that ORCHIDEE does not well simulate ET over grasslands and crops (Krinner et al., 2005) and CABLE has limitations simulating ET over wet regions (Zhang et al., 2016c).

5. Summary and outlook

In summary, we generated a monthly evapotranspiration (ET) dataset over China from 1982 to 2015 at a high resolution (0.1°) by integrating 826 site-months in-situ measurements covering all ecosystem types using MTE algorithms. We characterized the spatiotemporal patterns of ET in China over the past 30 years and compared them with existing global ET products. Our product reduced the large uncertainties in China's ET estimates. The main findings in this study include: (1) China's ET has increased significantly (10.7 mm yr^{-1} per decade, $p < 0.05$) over the past thirty years, with large spatial heterogeneity (78% areas increased and 22% areas decreased). (2) The increasing annual ET is caused by increasing precipitation, temperature and NDVI as well as decreasing relative humidity, while interannual variability of ET is impacted by the interannual variability of temperature, solar radiation and relative humidity. (3) ET products are subject to uncertainties in terms of the magnitude, spatial distribution as well as temporal variation, especially ET trend at local scale.

To further reduce the uncertainty of ET reconstructions, more direct observations of terrestrial ET covering wider geographical regions and longer measuring periods should be collected. Second, we need to focus on reducing uncertainties of driving factors used to constrain ET, such as precipitation, radiation, temperature, and vegetation indices (e.g., NDVI and LAI) (Fisher et al., 2008; Mu et al., 2011; Mueller et al., 2013; Badgley et al., 2015). Third, land surface models require numerous site-specific calibrated parameters to simulate ET processes (Rigden and Salvucci, 2015), yet we still have little knowledge on some key parameters and mechanisms involved (Mu et al., 2011).

Acknowledgements

This study was supported by the National Natural Science Foundation of China (41561134016), National Youth Top-notch Talent Support Program in China, the 111 Project, China (B14001).

Appendix A. Supplementary data

Supplementary material related to this article can be found, in the online version, at doi:https://doi.org/10.1016/j.agrformet.2018.04.020.

References

Badgley, G., Fisher, J.B., Jiménez, C., et al., 2015. On uncertainty in global terrestrial evapotranspiration estimates from choice of input forcing datasets**. J. Hydrometeorol. 16, 1449–1455.

Baldocchi, D., Falge, E., Gu, L., et al., 2001. FluxNET: a new tool to study the temporal and spatial variability of ecosystem-scale carbon dioxide, water vapor, and energy flux densities. Bull. Am. Meteorol. Soc. 82, 2415–2434.

Bastiaanssen, W.G.M., 2000. SEBAL-based sensible and latent heat fluxes in the irrigated Gediz Basin. Turk. J. Hydrol. 229, 87–100.

Chen, Y., Xia, J., Liang, S., et al., 2014. Comparison of satellite-based evapotranspiration models over terrestrial ecosystems in China. Remote Sens. Environ. 140, 279–293.

Chen, Y., Yang, K., He, J., et al., 2011. Improving land surface temperature modeling for dry land of China. J. Geophys. Res. Atmos. 116, D20104. http://dx.doi.org/10.1029/2011JD015921.
Decker, M., Or, D., Pitman, A., Ukkola, A., 2017. New turbulent resistance parameterization for soil evaporation based on a pore-scale model: impact on surface fluxes in CABLE. J. Adv. Model. Earth Syst. 9, 220–238.
Douville, H., Ribes, A., Decharme, B., Alkama, R., Sheffield, J., 2012. Anthropogenic influence on multidecadal changes in reconstructed global evapotranspiration. Nat. Clim. Change 3, 59–62.
Editorial Board of Vegetation Map of China, 2007. Chinese Academy of Sciences. Vegetation Map of the People's Republic of China (1:1000000) (Digital Version). Geology Press, Beijing, China.
Evaristo, J., Jasechko, S., McDonnell, J.J., 2015. Global separation of plant transpiration from groundwater and streamflow. Nature 525, 91–94.
Fisher, J.B., Tu, K.P., Baldocchi, D.D., 2008. Global estimates of the land-atmosphere water flux based on monthly AVHRR and ISLSCP-II data, validated at 16 FLUXNET sites. Remote Sens. Environ. 112, 901–919.
Gaucherel, C., Alleaume, S., Hély, C., 2008. The comparison map profile method: a strategy for multiscale comparison of quantitative and qualitative images. IEEE Trans. Geosci. Remote Sens. 46, 2708–2719.
Guimberteau, M., Ducharne, A., Ciais, P., Boisier, J.P., Peng, S., De Weirdt, M., Verbeeck, H., 2014. Testing conceptual and physically based soil hydrology schemes against observations for the Amazon Basin. Geosci. Model. Dev. 7, 1115–1136.
Huang, M., Piao, S., Sun, Y., et al., 2015. Change in terrestrial ecosystem water-use efficiency over the last three decades. Glob. Change Biol. 21, 2366–2378.
Jarvis, P.G., 1995. Scaling processes and problems. Plant. Cell Environ. 18, 1079–1089.
Jasechko, S., Sharp, Z.D., Gibson, J.J., et al., 2013. Terrestrial water fluxes dominated by transpiration. Nature 496, 347–350.
Jimenez, C., Prigent, C., Mueller, B., et al., 2011. Global intercomparison of 12 land surface heat flux estimates. J. Geophys. Res. 116, D02102. http://dx.doi.org/10.1029/2010JD014545.
Jung, M., Reichstein, M., Bondeau, A., 2009. Towards global empirical upscaling of FLUXNET eddy covariance observations: validation of a model tree ensemble approach using a biosphere model. Biogeosci. Discuss. 6, 5271–5304.
Jung, M., Reichstein, M., Ciais, P., et al., 2010. Recent decline in the global land evapotranspiration trend due to limited moisture supply. Nature 467, 951–954.
Jung, M., Reichstein, M., Margolis, H.A., et al., 2011. Global patterns of land-atmosphere fluxes of carbon dioxide, latent heat, and sensible heat derived from eddy covariance, satellite, and meteorological observations. J. Geophys. Res. Biogeosci. 116, G00J. http://dx.doi.org/10.1029/2010JG001566.
Kowalczyk, E.A., Wang, Y.P., Law, R.M., 2006. The CSIRO atmosphere biosphere land exchange (CABLE) model for use in climate models and as an offline model. CSIRO Mar. Atmos. Res. Pap. 13, 42.
Krinner, G., Viovy, N., de Noblet-Ducoudré, N., et al., 2005. A dynamic global vegetation model for studies of the coupled atmosphere-biosphere system. Glob. Biogeochem. Cycles 19, 1–33.
Kustas, W.P., Norman, J.M., 1996. Use of remote sensing for evapotranspiration monitoring over land surfaces. Hydrol. Sci. J. 41, 495–516.
Liu, J.G., Xie, Z.H., 2013. Improving simulation of soil moisture in China using a multiple meteorological forcing ensemble approach. Hydrol. Earth Syst. Sci. 17, 3355–3369.
Liu, J., Jia, B., Xie, Z., et al., 2016a. Ensemble simulation of land evapotranspiration in China based on a multi-forcing and multi-model approach. Adv. Atmos. Sci. 33, 673–684.
Liu, Y., Xiao, J., Ju, W., Xu, K., Zhou, Y., Zhao, Y., 2016b. Recent trends in vegetation greenness in China significantly altered annual evapotranspiration and water yield. Environ. Res. Lett. 11 (9). http://dx.doi.org/10.1088/1748-9326/11/9/094010.
Machiwal, D., Jha, M.K., 2006. Time series analysis of hydrologic data for water resources planning and management: a review. J. Hydrol. Hydromech. 54, 237–257.
Mao, J., Fu, W., Shi, X., Ricciuto, D.M., Fisher, J.B., et al., 2015. Disentangling climatic and anthropogenic controls on global terrestrial evapotranspiration trends. Environ. Res. Lett. 10 (9). http://dx.doi.org/10.1088/1748-9326/10/9/094008.
Miralles, D.G., van den Berg, M.J., Gash, J.H., et al., 2014. El Nino-La Nina cycle and recent trends in continental evaporation. Nat. Clim. Change 4, 122–126.
Moffat, A.M., Papale, D., Reichstein, M., et al., 2007. Comprehensive comparison of gap-filling techniques for eddy covariance net carbon fluxes. Agric. For. Meteorol. 147, 209–232.
Mu, Q., Heinsch, F.A., Zhao, M., et al., 2007. Development of a global evapotranspiration algorithm based on MODIS and global meteorology data. Remote Sens. Environ. 111, 519–536.
Mu, Q., Zhao, M., Running, S.W., 2011. Improvements to a MODIS global terrestrial evapotranspiration algorithm. Remote Sens. Environ. 115, 1781–1800.
Mueller, B., Hirschi, M., Jimenez, C., et al., 2013. Benchmark products for land evapotranspiration: LandFlux-EVAL multi-data set synthesis. Hydrol. Earth Syst. Sci. 17, 3707–3720.
Oleson, K.W., Lawrence, D.M., Gordon, B., et al., 2010. Technical Description of Version 4.0 of the Community Land Model (CLM), NCAR/TN-478 + STR. Natl. Cent. For Atmos. Res., Boulder, Colo.
Pan, S., Tian, H., Dangal, S.R.S., et al., 2015. Responses of global terrestrial evapotranspiration to climate change and increasing atmospheric CO_2 in the 21st century. Earth's Future 3, 15–35.
Piao, S., Mohammat, A., Fang, J., et al., 2006. NDVI-based increase in growth of temperate grasslands and its responses to climate changes in China. Glob. Environ. Change 16, 340–348.
Piao, S., Yin, G., Tan, J., et al., 2015. Detection and attribution of vegetation greening trend in China over the last 30 years. Glob. Change Biol. 21, 1601–1609.
Pinzon, J.E., Tucker, C.J., 2014. A non-stationary 1981-2012 AVHRR NDVI3g time series. Remote Sens. 6, 6929–6960.
Rahmani, V., Hutchinson, S.L., Harrington, J.A., et al., 2015. Analysis of temporal and spatial distribution and change-points for annual precipitation in Kansas. U. S. A. Int. J. Climatol. 35, 3879–3887.
Reichstein, M., Falge, E., Baldocchi, D., et al., 2005. On the separation of net ecosystem exchange into assimilation and ecosystem respiration: review and improved algorithm. Glob. Change Biol. 11 (9), 1424–1439.
Rigden, A.J., Salvucci, G.D., 2015. Evapotranspiration based on equilibrated relative humidity (ETRHEQ): evaluation over the continental U.S. Water Resour. Res. 51, 2951–2973.
Sellers, P.J., Dickinson, R.E., Randall, D.A., 1997. Modeling the exchanges of energy, water, and carbon between continents and the atmosphere. Science 275, 502–509.
Shi, X., Mao, J., Thornton, P.E., et al., 2013. Spatiotemporal patterns of evapotranspiration in response to multiple environmental factors simulated by the community land model. Environ. Res. Lett. 8, 24012. http://dx.doi.org/10.1088/1748-9326/8/2/024012.
Trenberth, K.E., Smith, L., Qian, T., et al., 2007. Estimates of the global Water budget and its annual cycle using observational and model data. J. Hydrometeorol. 8, 758–769.
Tucker, C., Pinzon, J., Brown, M., et al., 2005. An extended AVHRR 8-km NDVI dataset compatible with MODIS and SPOT vegetation NDVI data. Int. J. Remote Sens. 26, 4485–4498.
Ukkola, A.M., Pitman, A.J., Decker, M., et al., 2016. Modelling evapotranspiration during precipitation deficits: identifying critical processes in a land surface model. Hydrol. Earth Syst. Sci. 20, 2403–2419.
Ukkola, A.M., Prentice, I.C., 2013. A worldwide analysis of trends in water-balance evapotranspiration. Hydrol. Earth Syst. Sci. 17, 4177–4187.
Wang, K., Dickinson, R.E., 2012. A review of global terrestrial evapotranspiration: observation, modelling, climatology, and climatic variability. Rev. Geophys. 50, 1–54.
Wang, K., Dickinson, R.E., Wild, M., et al., 2010a. Evidence for decadal variation in global terrestrial evapotranspiration between 1982 and 2002: 2. Results. J. Geophys. Res. Atmos. 115, D20113. http://dx.doi.org/10.1029/2010JD013847.
Wang, Y.P., Law, R.M., Pak, B., 2010b. A global model of carbon, nitrogen and phosphorus cycles for the terrestrial biosphere. Biogeosciences 7, 2261–2282.
Wang, Y.P., Leuning, R., 1998. A two-leaf model for canopy conductance, photosynthesis and partitioning of available energy I: model description and comparison with a multi-layered model. Agric. For. Meteorol. 91 (1–2), 89–111.
Wang, Y.P., Kowalczyk, E., Leuning, R., et al., 2011. Diagnosing errors in a land surface model (CABLE) in the time and frequency domains. J. Geophys. Res. Biogeosci. 116, G01034. http://dx.doi.org/10.1029/2010JG001385.
Wei, Y., Liu, S., Huntzinger, D.N., Michalak, et al., 2014. The north american carbon program multi-scale synthesis and terrestrial model intercomparison project - Part 2: environmental driver data. Geosci. Model. Dev. 7 (6), 2875–2893.
Winslow, J.C., Hunt, E.R., Piper, S.C., 2003. The influence of seasonal water availability on global C3 versus C4 grassland biomass and its implications for climate change research. Ecol. Model. 163 (1–2), 153–173.
Yan, H., Wang, S.Q., Billesbach, D., et al., 2012. Global estimation of evapotranspiration using a leaf area index-based surface energy and water balance model. Remote Sens. Environ. 124, 581–595.
Yang, K., He, J., Tang, W., et al., 2010. On downward shortwave and longwave radiations over high altitude regions: observation and modeling in the Tibetan Plateau. Agric. For. Meteorol. 150, 38–46.
Yao, Y., Liang, S., Li, X., et al., 2017. Improving global terrestrial evapotranspiration estimation using support vector machine by integrating three process-based algorithms. Agric. For. Meteorol. 242, 55–74.
Zeng, Z., Piao, S., Li, L.Z.X., et al., 2017. Climate mitigation from vegetation biophysical feedbacks during the past three decades. Nat. Clim. Change 7, 432–436.
Zeng, Z., Piao, S., Lin, X., et al., 2012. Global evapotranspiration over the past three decades: estimation based on the water balance equation combined with empirical models. Environ. Res. Lett. 7, 14026. http://dx.doi.org/10.1088/1748-9326/7/1/014026.
Zeng, Z., Wang, T., Zhou, F., et al., 2014. A worldwide analysis of spatiotemporal changes in water balance-based evapotranspiration from 1982 to 2009. J. Geophys. Res. 119, 1186–1202.
Zhang, K., Kimball, J.S., Nemani, R.R., et al., 2010. A continuous satellite-derived global record of land surface evapotranspiration from 1983 to 2006. Water Resour. Res. 46, W09522. http://dx.doi.org/10.1029/2009WR008800.
Zhang, K., Kimball, J.S., Nemani, R.R., et al., 2015. Vegetation greening and climate change promote multidecadal rises of global Land evapotranspiration. Sci. Rep. 5, 1–9.
Zhang, K., Kimball, J.S., Running, S.W., 2016a. A review of remote sensing based actual evapotranspiration estimation. Wiley Interdiscip. Rev. Water 3 (6), 834–853.
Zhang, Y., Chiew, F.H.S., Peña-Arancibia, J., Sun, F., Li, H., Leuning, R., 2017. Global variation of transpiration and soil evaporation and the role of their major climate drivers. J. Geophys. Res. 122 (13), 6868–6881.
Zhang, Y., Peña-Arancibia, J.L., McVicar, T.R., et al., 2016b. Multi-decadal trends in global terrestrial evapotranspiration and its components. Sci. Rep. 6, 19124.
Zhang, Y., Zheng, H., Chiew, F., et al., 2016c. Evaluating regional and global hydrological models against streamflow and evapotranspiration measurements. J. Hydrometeorol. 17 (3), 160118112748006. http://dx.doi.org/10.1175/JHM-D-15-0107.1.
Zhou, X., Zhang, Y., Wang, Y., et al., 2012. Benchmarking global land surface models against the observed mean annual runoff from 150 large basins. J. Hydrol. 470–471, 269–279.
Zhu, Z., Piao, S., Myneni, R.B., et al., 2016. Greening of the earth and its drivers. Nat. Clim. Change 6, 791–795.